

Supplement of

Infrared-based retrieval of dust optical depth and coarse-mode effective size from collocated MODIS and CALIOP observations

Jianyu Zheng et al.

Correspondence to: Zhibo Zhang (zhibo.zhang@umbc.edu)

1 The *a priori* monomodal lognormal volume size distribution

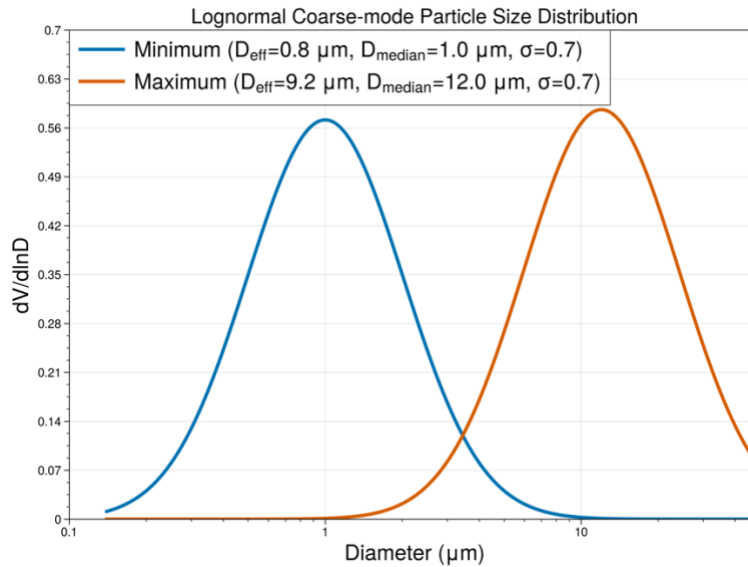


Figure S1: The assumed monomodal coarse-mode volume size distribution with the geometric volume median diameter ranging from 1.0 μm to 12.0 μm , the fixed standard deviation at 0.7, and the effective diameter ranging from 0.8 μm to 9.2 μm .

2 The refractive index assignment based on the dust source fractional contribution from DustCOMM

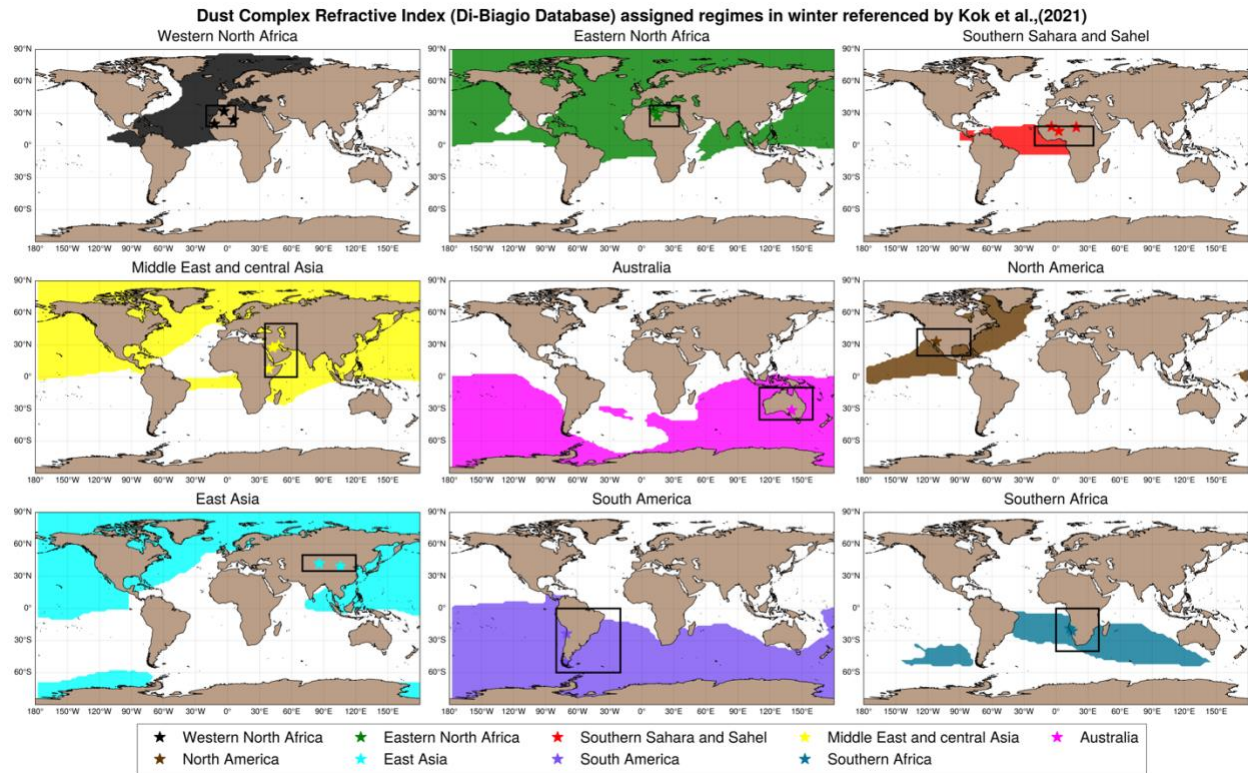


Figure S2: The assignment of the source region-resolved dust refractive indices from Di Biagio et al. (2017) is based on which of the nine main source regions provided a fractional contribution to SW DAOD that exceeds 0.1, which is shown here for winter based on the DustCOMM-2021 dataset.

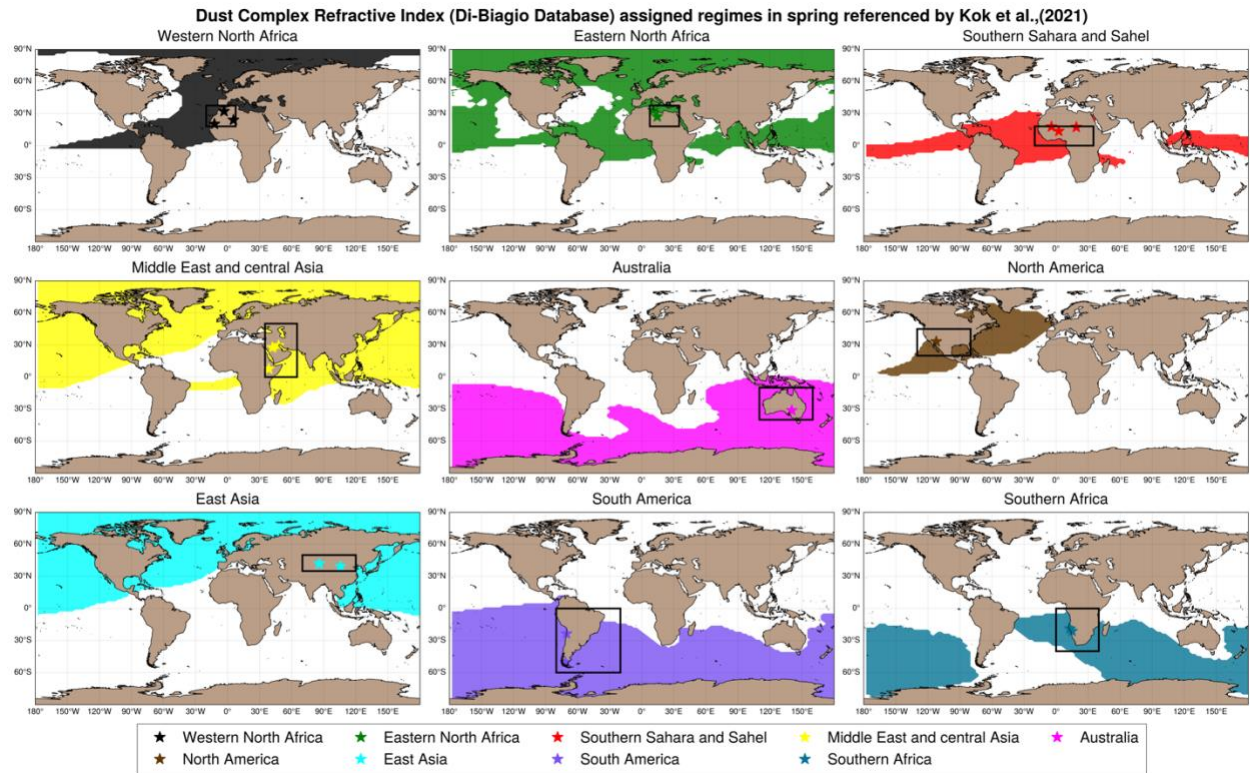


Figure S3: Same as Figure S2 but for spring based on the DustCOMM-2021 dataset.

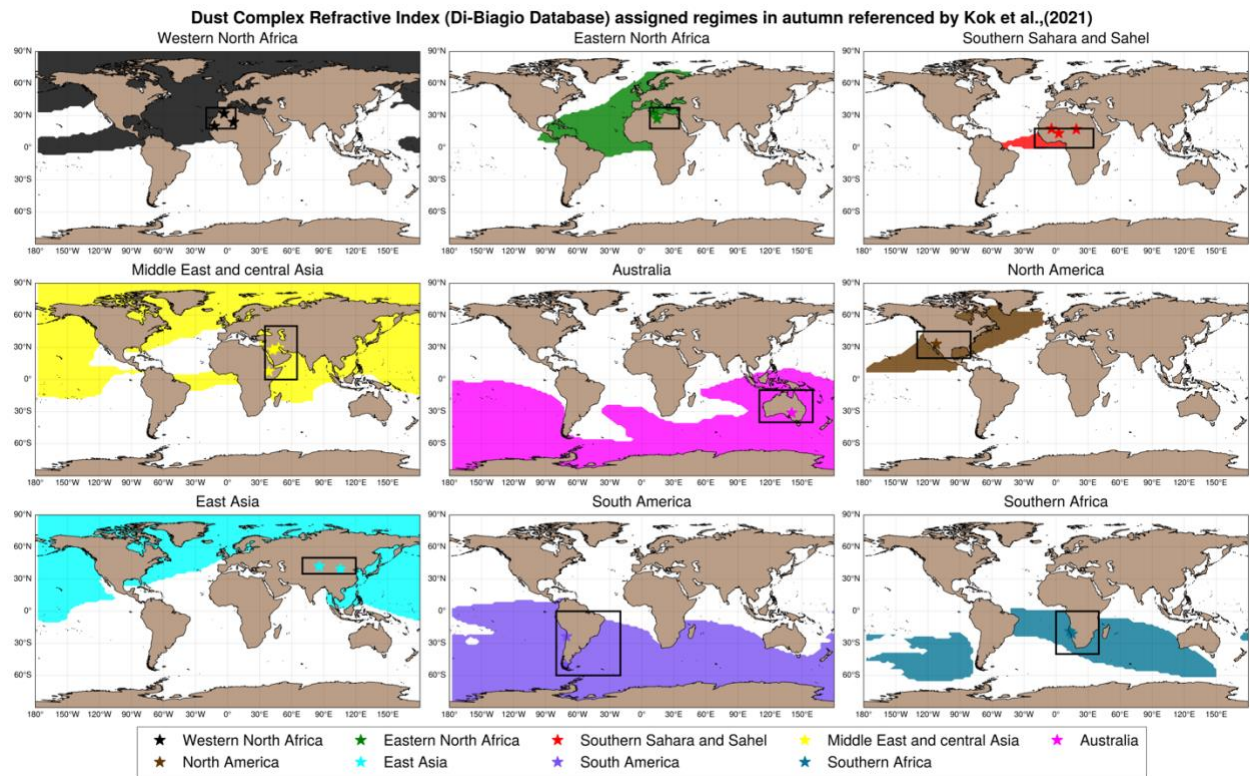


Figure S4: Same as Figure S2 but for autumn based on the DustCOMM-2021 dataset.

3 The sensitivity of TIR radiative signature to the σ of dust particle size distributions and dust refractive indices

Dust effective absorption in LW spectrum regarding to σ of PSD with Algeria RI

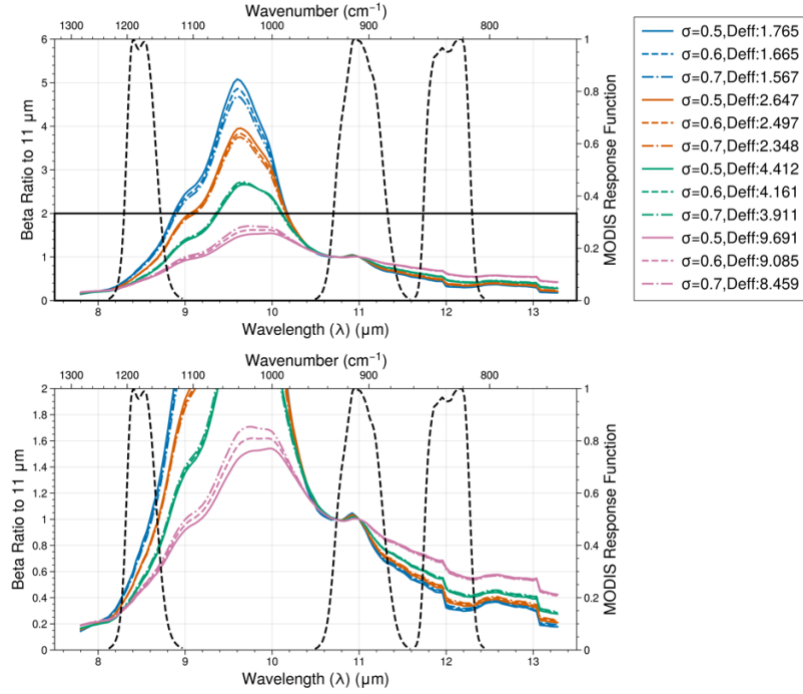


Figure S5: (a) The β -ratio to 11 μm calculated based on $D_m = 2 \mu\text{m}$ (blue), 3 μm (red), 5 μm (green) and 10 μm (pink) with three different σ (i.e., $\sigma = 0.5$ (real curves), 0.6 (dash curves), 0.7 (dot-dash curves)) of dust PSD and the Algeria dust RI from Di-Biagio Database within the TIR spectrum between 7.5 μm and 13.5 μm . (b) The zoom-in area of the black rectangle in (a).

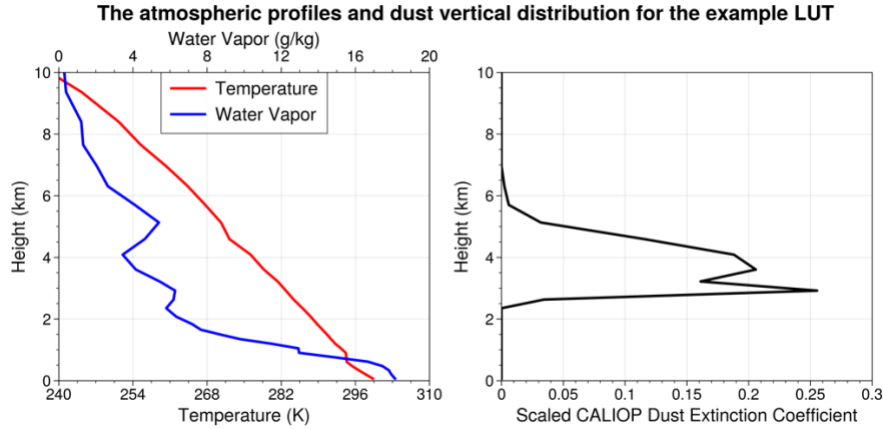


Figure S6: The atmospheric profile and dust vertical distribution used for building the LUT in Figure 4 and LUTs in Figures S7 and S8.

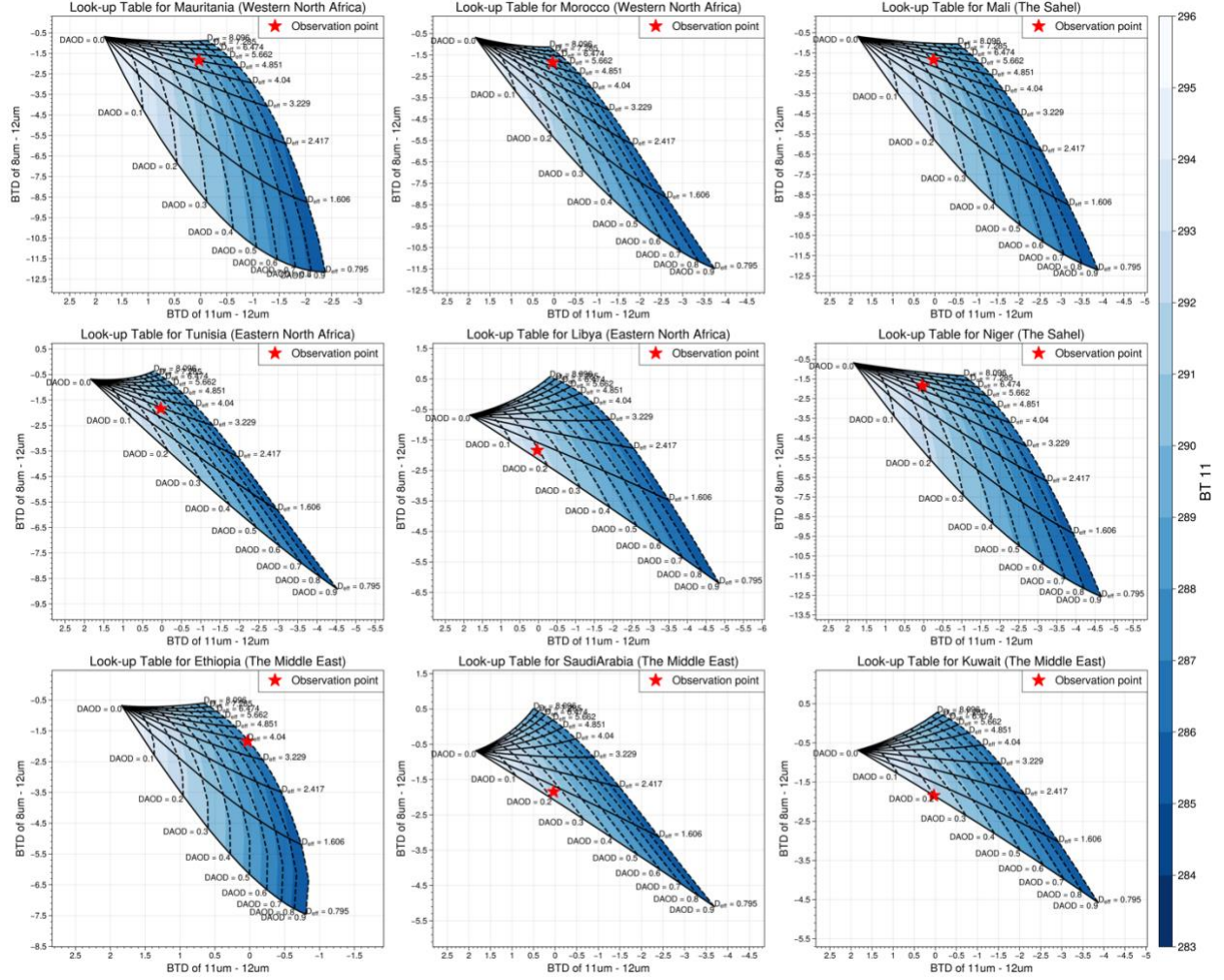


Figure S7: The example of the LUT of $BT_{D_{8-12}}$ (y-axis), $BT_{D_{11-12}}$ (x-axis) and BT_{11} (colour-filled contours) corresponding to DAOD at 10 μm ranging from 0.0 to 1.0 (dashed lines) and D_{eff} ranging from 0.8 μm to 9.0 μm (solid lines) and eighteen dust RIs except the Algeria RI (Figure 2a) from Di-Biagio Database. At DAOD = 0.0, the $BT_{D_{8-12}}$ and $BT_{D_{11-12}}$ correspond to the cloud-free clean scenario. The red dots represent an identical assumed observation point projected on the nine LUTs, leading to different retrieval solutions.

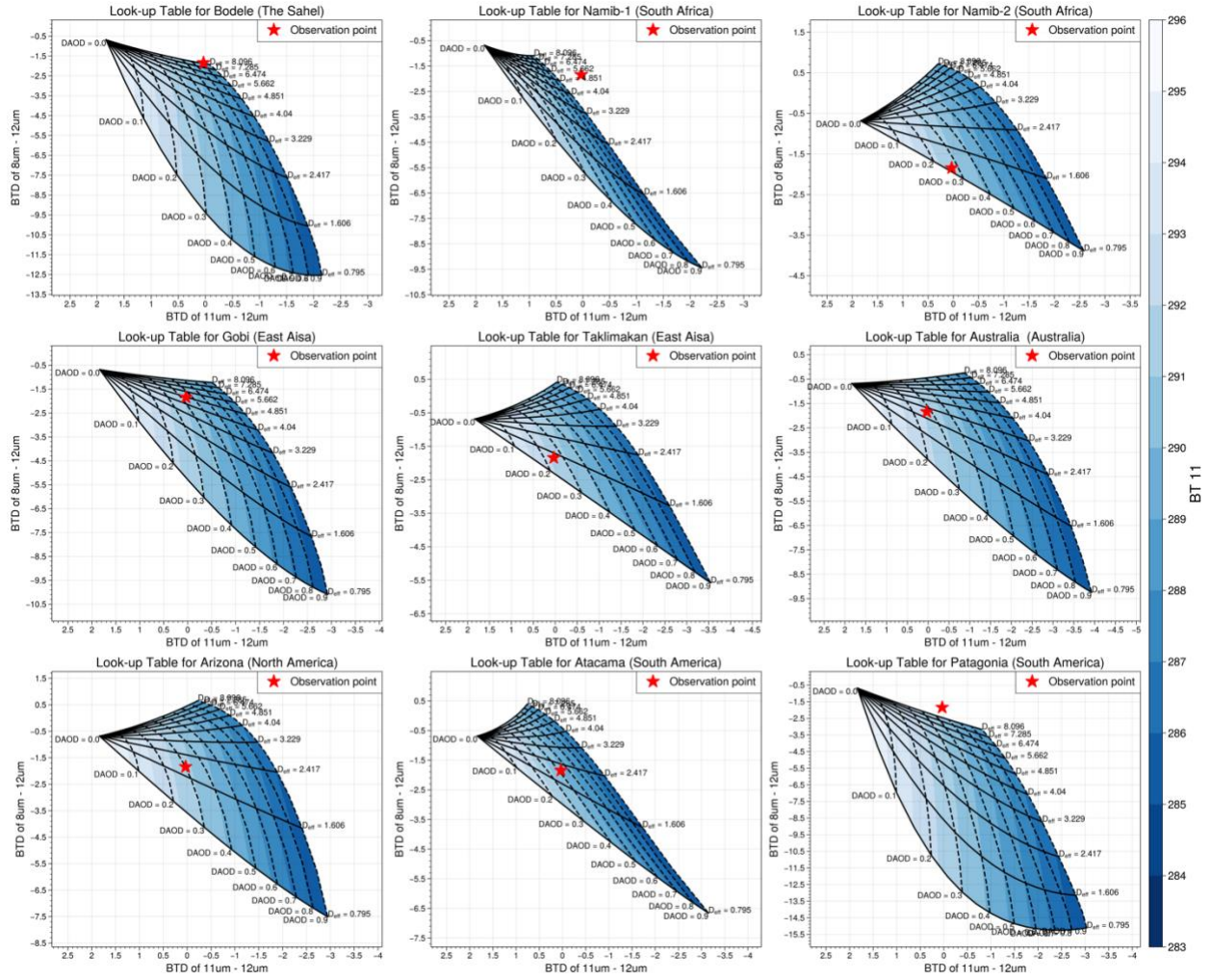


Figure S8: Continued as Figure S7.

4 The sample distributions of the retrieval from 2013 to 2017

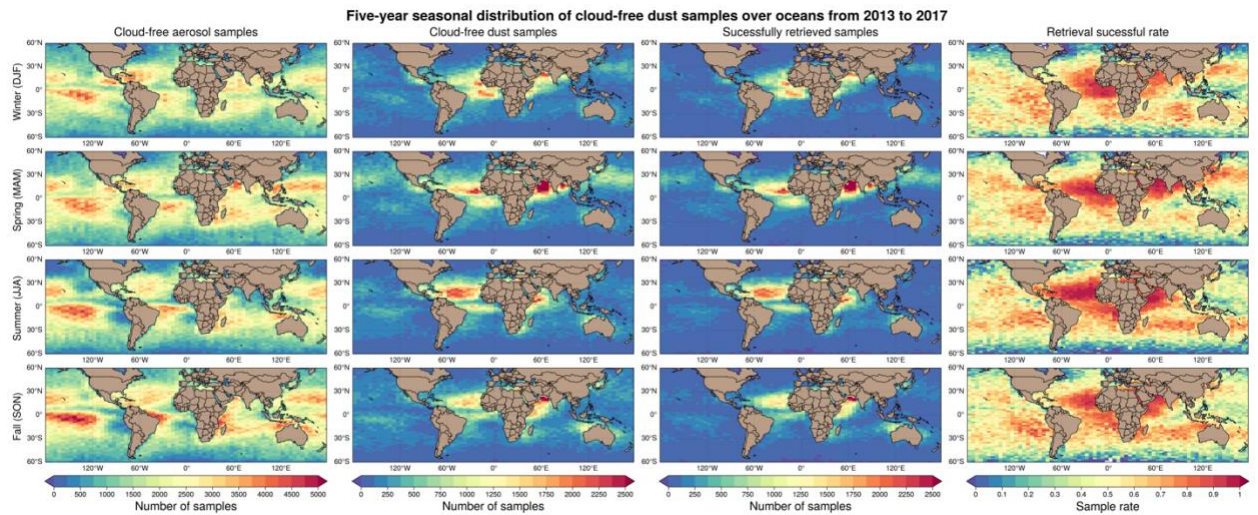


Figure S9: The five-year global seasonal distribution in a 5° longitude by 2° latitude resolution of the cloud-free aerosol samples ($N_{aerosol}$; left column), the cloud-free aerosol samples (N_{dust} ; middle-left column), the successfully retrieved samples ($N_{retrieval}$; middle-right column) and the retrieval success rate ($N_{retrieval} / N_{dust}$; right column). From the top row to the bottom presents seasons from winter to fall.